Article

Phosphate Removal from Polluted Water via Lanthanum-Modified Sludge Biochar

Yufan Jiang [1,2], Xiaojie Sun [1,2,*], Hongxia Zhang [1,2,*], Qian Li [1,2], Jingjing Mo [1,2], Meiyan Xing [3], Bin Dong [1,3] and Hongxiang Zhu [4,5]

1   Guangxi Key Laboratory of Environmental Pollution Control Theory and Technology, Guilin University of Technology, Guilin 541004, China; 2120220510@glut.edu.cn (Y.J.); lq1643136880@outlook.com (Q.L.); 1020210416@glut.edu.cn (J.M.); dongbin@tongji.edu.cn (B.D.)
2   Guangxi Collaborative Innovation Center for Water Pollution Control and Water Safety in Karst Area, Guilin University of Technology, Guilin 541004, China
3   School of Environmental Science and Engineering, Tongji University, Shanghai 200092, China; xingmeiyan@tongji.edu.cn
4   College of Light Industry and Food Engineering, Guangxi University, Nanning 530004, China; zhx@gxu.edu.cn
5   Modern Industry College of Ecology and Environmental Protection, Guilin University of Technology, Guilin 541004, China
*   Correspondence: sunxiaojie@glut.edu.cn (X.S.); zhx75@glut.edu.cn (H.Z.)

Abstract: Biochar has attracted attention for its capability to remove phosphorus (P) from wastewater. However, the poor dispersion and limited adsorption capacity of unmodified biochar prevent its wide usage in water remediation. Herein, sludge biochar was modified using lanthanum nitrate to improve the removal of P from aqueous solutions. Scanning electron microscopy (SEM), X-ray diffraction (XRD), Fourier transform infrared spectroscopy (FTIR), and X-ray photoelectron spectroscopy (XPS) were used to elucidate the modification and adsorption mechanisms of biochar. Furthermore, the adsorption performance of the modified biochar was determined through adsorption kinetics and isotherm model fitting. The results showed that the modification process successfully introduced lanthanum-containing functional groups into biochar and considerably improved the complexation performance and ion-exchange capacity. The maximum experimental adsorption capacity for phosphate was 140.237 mg/g at pH 3.0. The adsorption processes of the modified biochar accorded with the Freundlich adsorption isotherm model, which indicates the successful adsorption of phosphate onto the modified biochar via multilayer adsorption. The adsorption mechanism was dominated by chemisorption, which mainly involved inner-sphere complexation, precipitation, and electrostatic attraction. Meanwhile, the adsorption and desorption experiments demonstrated the satisfying recycling performance of the modified biochar and the 72.3% adsorption capacity retention after the sixth desorption cycle. The dynamic adsorption study revealed that the modified biochar had long sustainable treatment durations of 7.58 and 9.08 h at adsorbent dosages of 1 and 2 g, respectively, which proves the feasibility of using biochar as a cost-effective and efficient adsorbent for phosphate-polluted water.

Keywords: adsorption; phosphate; modified biochar; lanthanum; sludge

1. Introduction

Phosphorus (P) is an essential nutrient in aquatic ecosystems [1–3]; however, excess P levels can cause severe eutrophication, which threatens ecosystems and human health [4,5]. Therefore, to regulate the discharge standards for sewage, the discharge requirements for P emissions have become increasingly stringent [6,7]. In particular, the current maximum permissible P level for discharged effluents of wastewater treatment plants (WWTPs) is 0.5 mg/L [8]. Hence, P levels must be reduced and controlled [8–10].

P may be removed from water through various techniques, including membrane separation, ion exchange, chemical precipitation, and electrocoagulation [11,12]. However, the unstable separation effect and high energy consumption limit the practical application of these methods [13,14]. In comparison, phosphate removal via adsorption technology is considerably promising. This process has the advantages of easy application, high removal efficiency, and cost effectiveness [15,16]. However, certain commonly used adsorbents, such as minerals and carbon compounds, which generally have low renewability or pose biodegradation difficulties, can also cause secondary pollution [17,18]. In addition, the majority of traditional adsorbents exhibit poor adsorption or high operation expenses. Therefore, an effective, affordable, and ecologically safe adsorbent must be created for the removal of phosphates from wastewater.

The rapid development of the urban economy has resulted in the generation of enormous quantities of municipal sewage sludge waste [19]. Sewage sludge waste contains high concentrations of nitrogen, P, organic micropollutants, heavy metals, and pathogens, which pose a major threat to human health and the environment if left untreated [20]. As a result, the treatment and reuse of sewage sludge have increasingly become the focus of attention in recent years [19,21]. To meet increasing population demands, a cost-effective and environmentally friendly disposal method must be development. Common methods used in sewage sludge treatments in developing countries, such as incineration and landfilling, cause secondary environmental pollution [19,22]. By contrast, thermal treatment, which is an economical and environmentally friendly method for sewage sludge recycling, enables the conversion of sewage sludge waste into functional biochar and valuable biofuels [23].

Biochar is a type of carbon-rich, porous adsorption material widely used in wastewater treatment and pollution remediation because of its exceptional structural qualities, abundant supplies, environmental friendliness, recyclability, and affordability [24–26]. Therefore, the thermal treatment of sewage sludge waste to yield biochar is important, as its aromatic hydrocarbon surface and oxygen-containing groups can be used to attain effective phosphate adsorption from wastewater and reduce the leaching of heavy metals, organic pollutants, and pathogens in sewage sludge products into soil and water for utilizing sewage sludge waste resources. Nevertheless, the poor dispersion and limited adsorption capacity of unmodified biochar prevent its wide application in water remediation [27,28]. Therefore, further modifications of sewage sludge biochar (SBC) are essential for its improved performance.

Given the high affinity of phosphate for metal oxides and its reaction with them to produce stable metal phosphates, metal-modified adsorbents are often used for phosphate removal [29]. Lanthanum (La) is an environmentally friendly and benign rare earth element [30,31], which has an abundant content and is inexpensive compared with other rare earth materials [32]. Meanwhile, chemical bonds between La and phosphate are stronger than those between phosphate and other metallic elements, such as aluminum and iron [33]. La-containing materials have garnered considerable attention for P removal because of their superior stability in aqueous solutions and outstanding adsorption selectivity. Fang et al. (2018) used a new magnetically recoverable magnetite/lanthanum hydroxide [M-La(OH)$_3$] for phosphate retention and recovery from lakes, demonstrating an adsorption capacity of up to 52.7 mg-P/g at pH 7.0 in water. La exhibits excellent selectivity, forms strong ionic bonds between La (III) and phosphate, and achieves good stability in aqueous solutions [34]. Min et al. (2019) synthesized a novel La-doped UiO-66, in which 0.2La-UiO-66 exhibited a high phosphate adsorption capacity, with the maximum adsorption capacity reaching 348.43 mg·g^{-1}. La modification increased the number of exposed adsorption sites and improved the phosphate adsorption of adsorbents [35].

Moreover, the addition of La may cause the biochar surface to become substantially less negatively charged; thus, the repulsion between the phosphate and biochar surface is weakened, increasing the likelihood of collisions [36]. Therefore, La-modified biochar can exhibit improved phosphate removal capacity from water. Therefore, in this study, SBC was synthesized through low-temperature oxygen-limited pyrolysis and was further

modified with lanthanum nitrate to form La-modified sludge biochar (LaSBC). The effects of the starting dose, solution pH, contact duration, and phosphate initial concentration on the adsorption process were investigated. The adsorption mechanism was discussed, together with the investigation of adsorption isotherms, kinetics, and thermodynamics. Furthermore, the dynamic adsorption capacity of adsorbents for actual wastewater in a fixed-bed column was evaluated. Thus, an innovative and cost-effective LaSBC using lanthanum nitrate as a modifier, proposed in this study, will provide a foundation for the modification of inexpensive and highly effective adsorbents.

2. Materials and Method

2.1. Preparation of Materials

SBC was produced via a low-temperature limited-oxygen pyrolysis. The dewatering sludge samples were collected from a sewage treatment plant in Guangxi, China, and then dried at 105 °C for 24 h. The dried sludge was ground and passed through a 120-mesh sieve. The sieved sludge powder was pyrolyzed in a tubular quartz furnace (SK2-6-12, Zhongyang Machinery Factory, Zhengzhou, China) at a rate of 10 °C/min to 600 °C, held at the target temperature for 3 h, surrounded by nitrogen gas [37,38], and then cooled to room temperature. The material acquired was labeled SBC.

The LaSBC was produced as follows: the SBC and analytical-grade La nitrate hexahydrate ($La(NO_3)_3 \cdot 6H_2O$) were dissolved in 40 mL ultrapure water at a 1:2 mass ratio. A magnetic stirrer was used to constantly agitate the mixture for 3 h at room temperature. When the solid had fully settled, the supernatant was drained off. After drying at 50 °C for 12 h and washing with ultrapure water, the LaSBC was finally produced.

2.2. Material Characterization

The surface morphology of various samples was determined via scanning electron microscopy (SEM; JSM-7900F, JEOL Ltd., Akishima, Japan). The elemental distribution of the adsorbent was analyzed using a field emission scanning electron microscope–energy-dispersive spectrometry (EDS; HitachiS-4800, Hitachi High Technology, Akishima, Japan). The surface functional groups of various samples before and after phosphate adsorption were investigated using Fourier transform infrared spectroscopy (FTIR; Nicolet Nexus 470, GMI-Technology Solutions, Phoneix, AZ, USA) in the 4000–500 cm^{-1} range. X-ray photoelectron spectroscopy (XPS; ESCALAB 250xi, Thermo Fisher Scientific, Waltham, MA, USA) was employed to analyze changes in functional groups and surface elemental contents. X-ray diffraction (XRD; X'Pert³ Powder, DKSH Group, Zurich, Switzerland) was utilized to determine the surface crystal structure of the samples. Further, the point of zero charge (pH_{pzc}) of various samples was ascertained via a zeta potential analyzer.

2.3. Batch Adsorption

Stock solutions containing 1000 $mg \cdot L^{-1}$ P(V) were prepared by dissolving potassium dihydrogen phosphate (KH_2PO_4) in ultrapure water. The stock solutions were then diluted to prepare the phosphate solutions required for the subsequent studies. The pH in this experiment was adjusted by adding 0.1 $mol \cdot L^{-1}$ HCl or NaOH. The entire adsorption process was performed in the oscillator of a thermostatic incubator.

Adsorption kinetics and isotherm models were used to investigate the overall interaction between phosphate and the adsorbents. The effects of the environmental factors (pH and adsorbent dosage) on the adsorption of phosphate on LaSBC were explored in this study. All experiments were repeated thrice. The operation steps of bath adsorption, calculation, and the fitting of graphs are described in the Supplementary Materials.

2.4. Adsorption and Desorption Experiments

For adsorption experiments, a 250 mL beaker was filled with a 140 mL 100 $mg \cdot L^{-1}$ phosphate solution, and 0.7 g LaSBC was added to it, and the resulting mixture was shaken

at 25 °C for 24 h. After filtration, the concentration of P in the supernatant liquid was determined and q_e was calculated.

For desorption experiments, filtered LaSBC was washed with ultrapure water for the removal of residual phosphate solutions, and adsorbents were subsequently dried in a drying oven at 50 °C for 12 h. The obtained product is the material, adsorbed once. Subsequently, 140 mL 0.2 mol·L^{-1} NaCl solution was mixed with 0.7 g of the material adsorbed once in 250 mL beakers. In addition, desorption was performed via constant shaking at 25 °C and 200 r·min^{-1} for 24 h. The filtered adsorbent, which is the material recycled once, was washed with ultrapure water until the pH became constant and dried. The LaSBC was recycled six times to assess the recyclability of the adsorbents.

2.5. Fixed-Bed Column Experiments

To determine the dynamic adsorption capacity of the adsorbents, we used a plexiglass column with an inner diameter of 10 mm and a height of 100 mm as a fixed-bed column reactor. Continuous fixed-bed column experiments were performed using an 8 cm deep fixed-bed column with various adsorbent amounts (1 and 2 g). The P removal effect of the modified biochar bed was studied at a certain flow rate (5 mL·min^{-1}) and the phosphate concentration (3.08 mg P/L) used in WWTPs. Dynamic adsorption involved the use of a peristaltic pump to pump the phosphate solution upward through the column and the collection of 5 mL samples at a given time interval for its analysis.

3. Results and Discussion

3.1. Material Characterization

The SEM characterizations of the SBC and LaSBC are displayed in Figure 1a–c. In addition, the EDS image of the LaSBC is presented in Figure 1d. Figure 1a shows a comparatively uniform block structure with a smooth surface and no holes, which resulted from the preservation of a substantial amount of ash and volatiles at a low preparation temperature [39]. After the modification with La, this smooth block structure was converted into irregular thick lumps (Figure 1b). The surface of the LaSBC contained abundant layered pores with numerous rough protuberances and grooves, demonstrating the effective grafting of La onto the LaSBC surface. This La grafting could also be directly proven by the presence of La in the EDS image (Figure 1d). Fine pore structures were well developed on the LaSBC surface after the loading of La^{3+}. The increase in fine pore structures provided more active sites for phosphate adsorption. After phosphate adsorption, the LaSBC surface was clustered, and the pores were completely occupied by phosphate (Figure 1c).

The FTIR spectra primarily represent changes in functional groups [40]. Figure 2 displays the FTIR spectra of LaSBC before and after adsorption. The peaks at 3430 and 1399 cm^{-1} can be attributed to the stretching vibrations of –OH [29,41], and those at 1633 and 1034 cm^{-1} can be associated with the C=C stretching vibration of the aromatic rings and the C–O stretching vibration, respectively [42–45]. The LaSBC spectra show an increase in the intensity and a shift in their –OH peaks compared with the SBC spectrum, suggesting the existence of several –OH groups that effectively adsorb phosphate [46]. Two distinct bands are observed at ~766 and ~711 cm^{-1} when comparing the FTIR spectra of SBC and LaSBC, which are characteristics of La–OH bond vibrations [47]. Moreover, the absorption peaks at 1461 and 1337 cm^{-1} are related to the vibration mode of the NO$_3^-$ anion in the feedstock La(NO$_3$)$_3$. After phosphate adsorption, the bands at 621 and 538 cm^{-1} are attributed to O–P–O bending vibrations [48,49]. Furthermore, a new peak at 593 cm^{-1} in the LaSBC-P spectrum originates from the La-O coordination between the active La site and oxygen anion in the phosphate molecule [47,50]. The observed alterations can be attributed to the phosphate-active La site reaction, which signifies the effective loading of La groups onto the SBC surface after La modification.
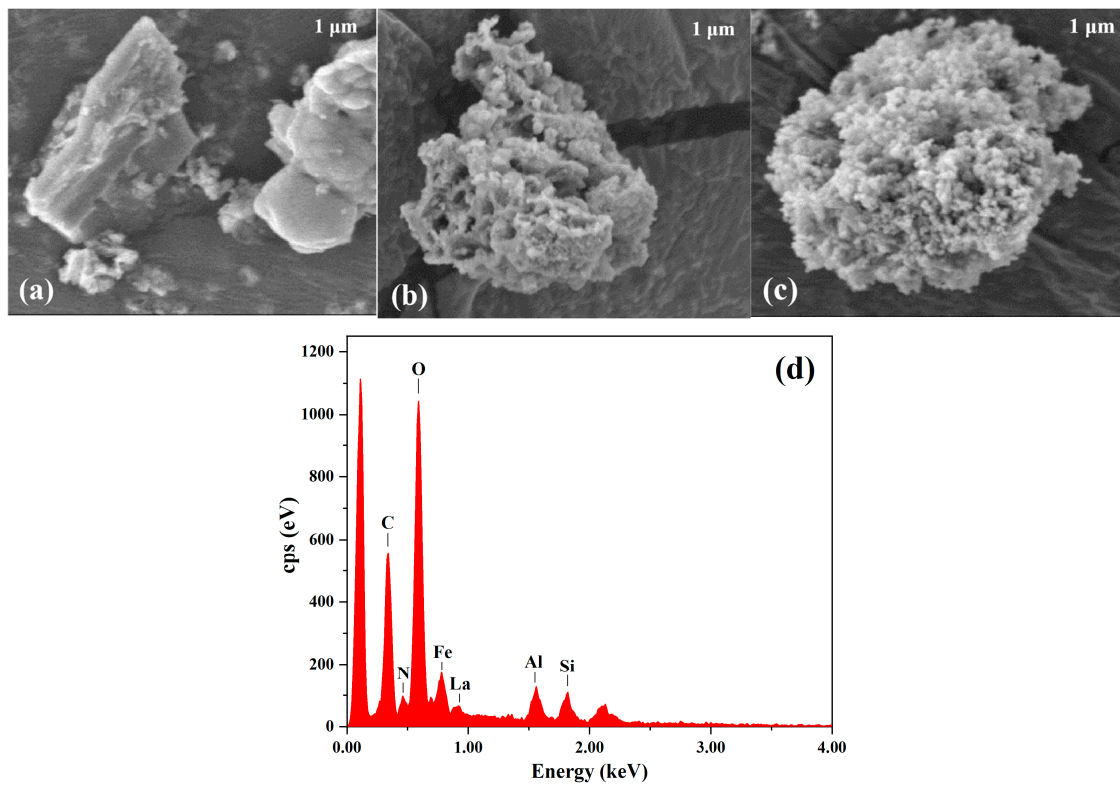
Figure 1. SEM images of SBC (**a**), LaSBC (**b**), and LaSBC-P (**c**), and EDS image of LaSBC (**d**).
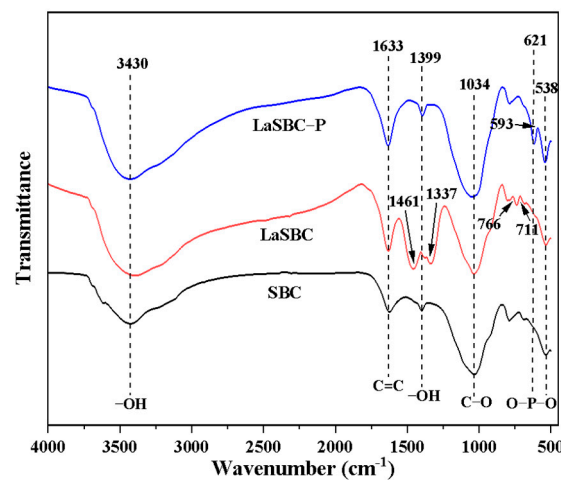

Figure 2. FTIR spectra of SBC, LaSBC, and LaSBC-P.

Additional information regarding the degree of crystallinity and material structure of the biochar materials was revealed by the XRD spectra. The XRD spectra of LaSBC and LaSBC-P (Figure 3) showed diffraction peaks at 13.238°, 18.901°, 20.917°, 31.240°, and 36.594°, which can be confidently matched with the characteristic peaks of La(OH)$_3$ [51]. Remarkably, the diffraction peaks corresponding to crystalline carbon structures, such as cellulose and lignin, were detected at a 2θ 26.662° [39,52]. This LaSBC peak was comparatively weaker than that of SBC, most likely because the heavier La^{3+} cations increased the absorption of X-ray radiation. Such a mechanism implies that lanthanide atoms are more effective at the diffusion of X-ray energy compared with sodium cations in biochar. After the exchange of Na$^+$ with La^{3+}, the electron density distribution varied dramatically. This condition resulted in the variation in beam interference, which reflects the relative intensities of individual reflections [53].
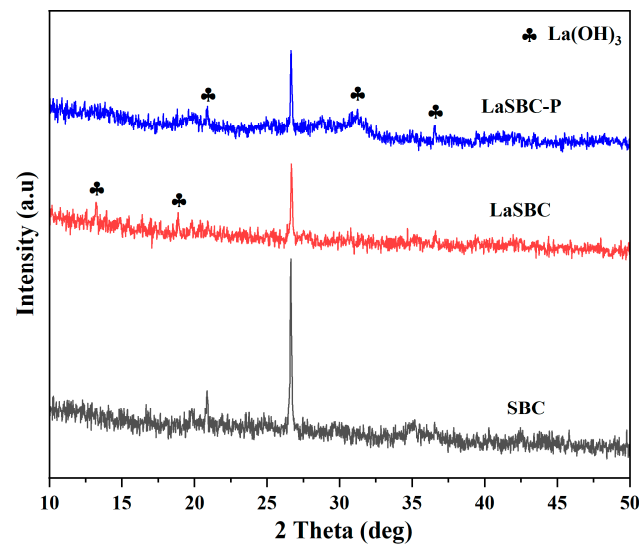
Figure 3. XRD spectra of SBC, LaSBC, and LaSBC-P.

XPS examination was performed to investigate changes in elements and chemical states on the LaSBC surface during adsorption (Figure 4). The peak of P 2p, which was clearly detected in LaSBC-P at a binding energy of 133.61 eV, confirmed the effective adsorption of phosphate on LaSBC.
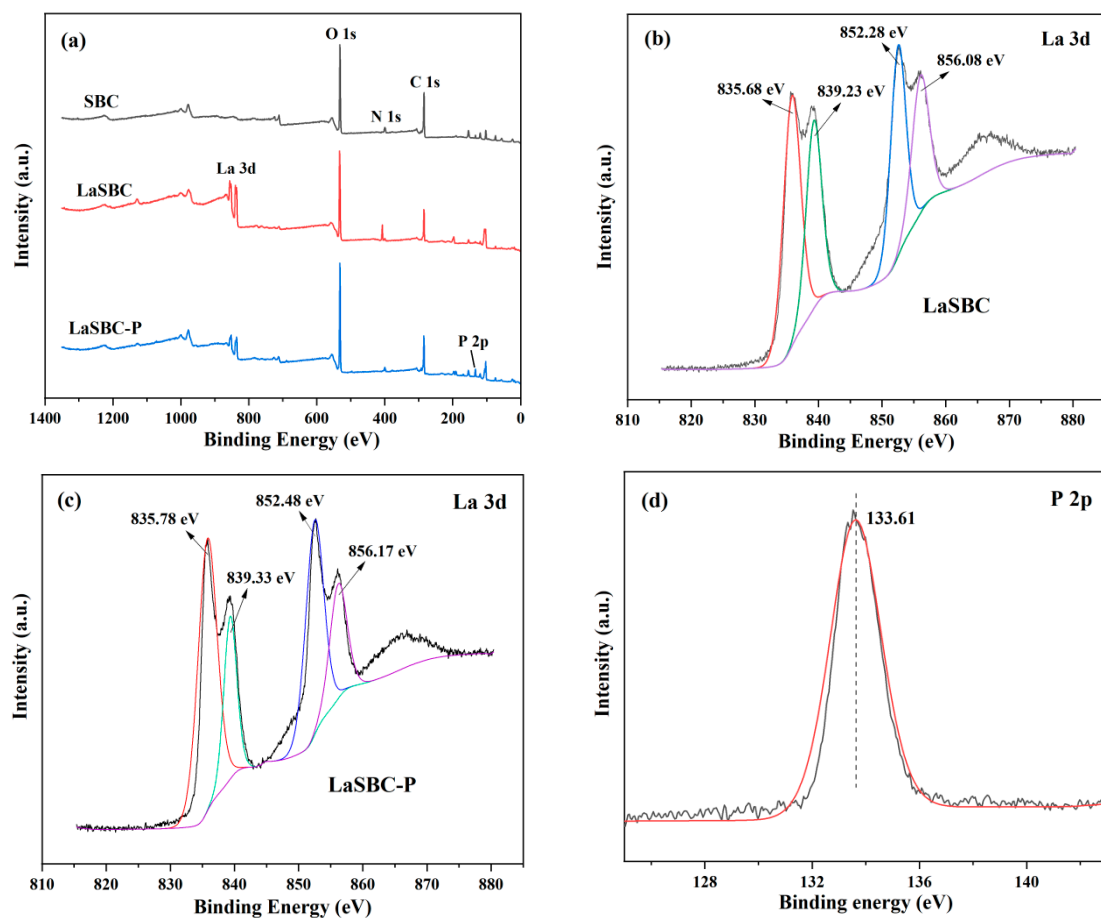

Figure 4. XPS spectra of LaSBC before and after adsorption. Full-spectrum diagram, (**a**) XPS spectra of La3d (**b**,**c**) before and after adsorption, and XPS spectra of P 2p (**d**) after adsorption.

3.2. Effect of Environmental Parameters

3.2.1. Effect of pH

The solution pH influences the surface charge properties of the adsorbent, thereby changing the interaction between the adsorbent and adsorbate and enabling the determination of the main types of phosphate (including H_3PO_4, $H_2PO_4^-$, HPO_4^{2-}, and PO_4^{3-}) [36,54]. Figure 5a illustrates the effect of pH on the phosphate absorption on SBC and LaSBC. The adsorption capacity (q_e) and removal rate of LaSBC in the pH 3–11 range were considerably improved compared with those of the SBC. In an acidic environment, the capability of the LaSBC to adsorb phosphates increased with an increase in the pH from 3 to 5. Neutral H_3PO_4 was the predominant phosphate species in low-pH solutions (pH < 3). Furthermore, it exhibited poor binding to the adsorption sites of LaSBC, due to the absence of ion exchange and electrostatic forces during the removal process. Meanwhile, the main phosphate species transformed into $H_2PO_4^-$ and HPO_4^{2-} at a pH between 5 and 7, and protonation left adsorbent surfaces positively charged. As a result, phosphate species were adsorbed onto the biochar via ion exchange and electrostatic forces. The maximum removal efficiency of LaSBC reached 99.06% at pH 5. The ion exchange and electrostatic interactions were less pronounced in an alkaline environment because of the substantial competition between hydroxide and phosphate and the deprotonation of the adsorbent surface. The electrostatic attraction between anions and adsorbents weakened with an increase in the OH^- concentration [53]. Further, the precipitation of La(III) hydroxide impeded LaSBC adsorption at pH 11.
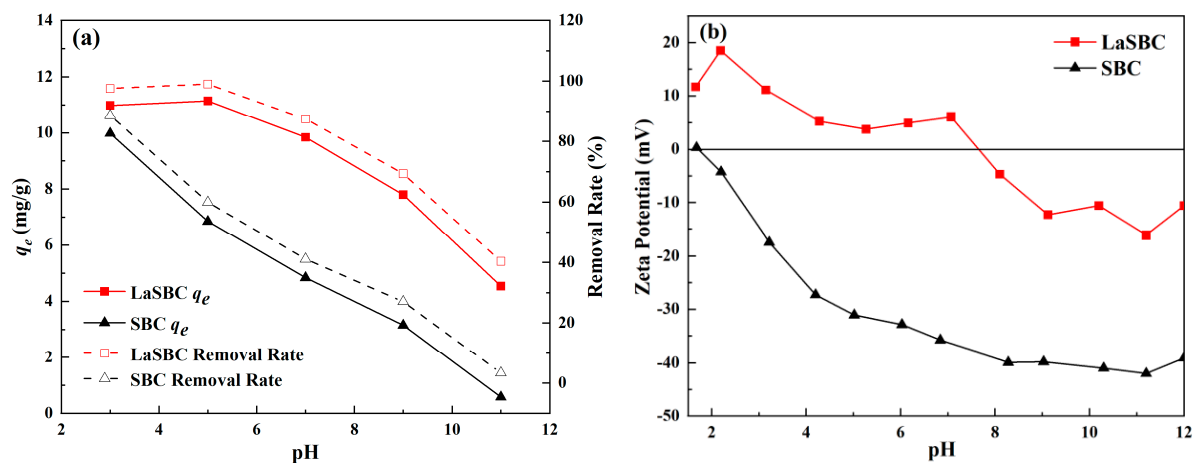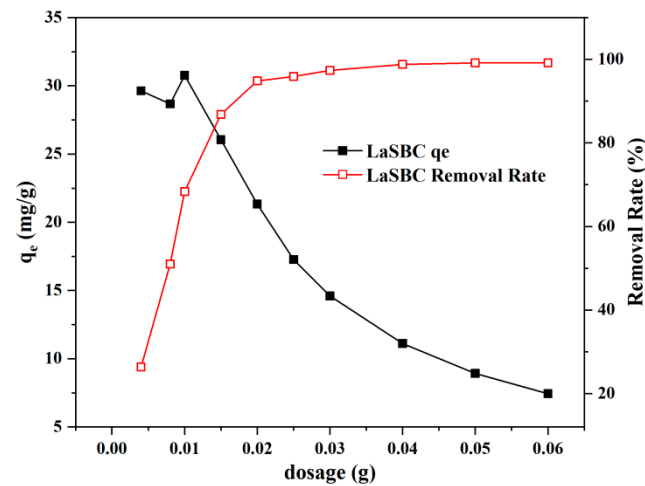

Figure 5. Effect of pH on the phosphate adsorption capacities and removal rate of SBC and LaSBC (**a**): zeta potential of SBC and LaSBC before phosphate sorption at various pH levels (**b**).

As a result of zeta potential changes, the surface charge of the LaSBC was altered dramatically with pH (Figure 5b). Over a broad pH range, the electronegativity of the LaSBC was lower than that of the SBC, indicating that the addition of La likely decreased the negative charge on the SBC surface via the formation of metal oxides on the surface [11,55]. Given the decrease in the negative charge, phosphate adsorption improved due to a reduction in the electrostatic repulsion between the biochar and anions [11]. However, in an extremely alkaline environment (pH 11), the electronegativity of the SBC and the LaSBC was incredibly high, which revealed that excessively alkaline surroundings negatively influence phosphate adsorption [11].

3.2.2. Effect of Adsorbent Dosages

The influence of LaSBC dosage on the adsorption process is presented in Figure 6. With an increase in adsorbent dosage from 0.004 to 0.06 g, the adsorption capacity (q_e) of the LaSBC dropped from 30.77 mg/g to 7.44 mg/g under the same starting phosphate concentration of 30 mg/L. However, the percentage removal of phosphate improved

from 68.37% to 99.17%. This result may be due to the quantity of active sites on the adsorbent and that were accessible for the adsorption process. The active sites accessible for phosphate adsorption increased with the increase in adsorbent dosage, which allowed for the adsorption of more phosphate and led to a better removal efficiency. As the amount of adsorbate in the solution was fixed, a decrease in the saturation of these active sites with phosphate occurred concurrently with this rise in active sites, which resulted in the observed decrease in q_e values [56].

Figure 6. Effect of dosage on phosphate adsorption capacities and removal rate of LaSBC.

3.3. Adsorption Kinetics

To better understand the adsorption process, we used several adsorption models for investigating the adsorption behavior of adsorbents (Figure 7). The reversible physical adsorption process is commonly described using a pseudo-first-order model, while the chemisorption process between an adsorbent and an adsorbate is explained via a pseudo-second-order model [57].
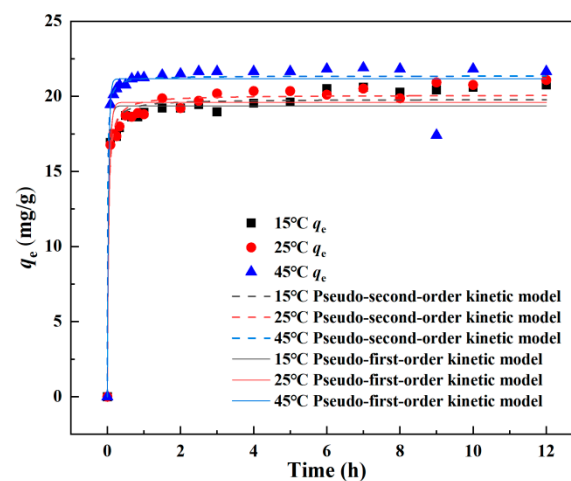
Figure 7. Kinetic process for phosphate adsorption on LaSBC.

Table S1 displays the fitting results obtained using the pseudo-first-order and pseudo-second-order kinetic models. The coefficient of determination (R^2 = 0.978, 0.979, and 0.961, respectively) of the pseudo-second-order kinetic model at 15 °C, 25 °C, and 45 °C was higher than that of the pseudo-first-order kinetic model (R^2 = 0.951, 0.946, and 0.958, respectively), indicating that chemisorption was predominant in phosphate adsorption on LaSBC. Additionally, the adsorption rate was controlled by the number of unoccupied sites

on the LaSBC. The primary cause for this phenomenon was that a significant number of La-based surface active sites was created following La doping, which paved the way for the chemical adsorption process [52].

3.4. Adsorption Isotherms

Phosphate adsorption from aqueous solutions on the biochar surface is described mathematically using the Langmuir or Freundlich isotherm, which facilitates the analysis of the adsorbent–adsorbate interaction and the structural properties of the adsorption layer [58]. The fitting curve of unary systems are shown in Figure 8, and the model parameters are listed in Table 1. The Langmuir model assumes the single-layer adsorption of the adsorbate on adsorbents, while the Freundlich model implies multilayer adsorption. Table 1 shows the multilayer adsorption of phosphate on the LaSBC surface, with the fitted R^2 of the Freundlich model for phosphate adsorption at 15 °C, 25 °C, 35 °C, 45 °C, and 65 °C being greater than those of the Langmuir model. As a result, the adsorption of phosphate onto LaSBC was heterogeneous, including interactions between adsorbed molecules, and an uneven surface energy [59,60]. The affinity of the adsorbate for the adsorbent is determined using the heterogeneity factor ($1/n$): the closer the factor is to zero, the stronger the affinity [58]. According to Table 1, the adsorbent had a sufficient adsorption capacity for phosphate, as the values of $1/n$ were less than one.
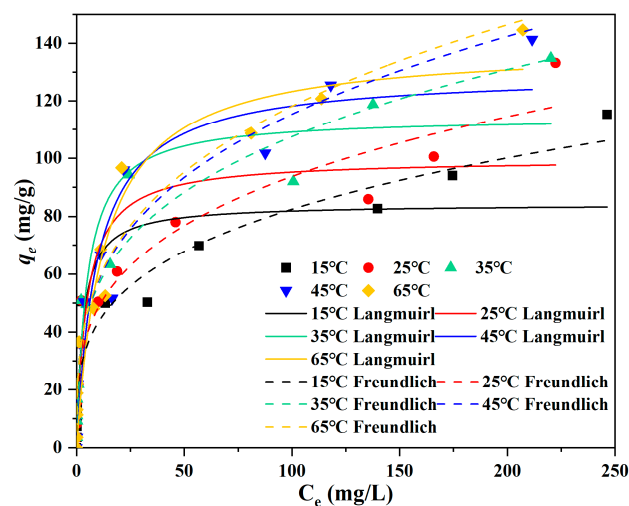

Figure 8. Isotherm process for the phosphate adsorption of LaSBC.

Table 1. Isotherm parameters for the phosphate adsorption of LaSBC.

Samples	Langmuir			Freundlich		
	Q_m (mg/g)	K_L (L/g)	R^2	K_F (L/g)	$1/n$	R^2
LaSBC 15 °C	84.249	0.346	0.848	22.670	0.280	0.941
LaSBC 25 °C	99.910	0.213	0.871	24.876	0.288	0.940
LaSBC 35 °C	114.647	0.206	0.922	29.111	0.284	0.943
LaSBC 45 °C	130.314	0.103	0.905	28.458	0.304	0.952
LaSBC 65 °C	140.237	0.077	0.924	28.347	0.310	0.960

As can be seen from Figure 8, the adsorption capacity of LaSBC rose with an increase in the phosphate initial concentration. This condition might have resulted from the high phosphate concentration, associated with a high driving-force concentration gradient [61]. In addition, more phosphate ions mean more opportunities for adsorbent capture. Furthermore, when the adsorption temperature increased from 15 °C to 65 °C, the adsorption capacity of the adsorbent for phosphate gradually increased, indicating that an elevated temperature is conducive for phosphate removal. This is because an increase in temperature

accelerates the diffusion rate of phosphate to the active sites on the LaSBC surface [40]. As shown in Table 1, according to the Langmuir model results, the maximum adsorption capacities of LaSBC toward phosphate were 84.249, 99.910, 114.647, 130.314, and 140.237 mg/g at the adsorption temperatures of 15 °C, 25 °C, 35 °C, 45 °C, and 65 °C, respectively. This result indicates that phosphate adsorption by LaSBC is an endothermic process [62].

The maximum capacity of LaSBC at 65 °C of 140.237 mg/g was determined using the Langmuir model. The greater ion mobility in the solution and increased likelihood of adsorption sites colliding with phosphate ions accounted for the enhanced adsorption capacity at higher temperatures [36]. The P adsorption capacity of LaSBC is better than the majority of other previously published metal-modified sludge adsorbents. Specific metal-modified adsorbents and their values are listed in Table 2.

Table 2. Comparison of P adsorption capacity of various metal-modified sludge biochars.

Biochar	Q_m (mg/g)	References
La-modified sludge biochar (LaSBC)	140.237	This study
Alkaline sludge biochar	42.51	[63]
Calcium-containing paper-sludge-based biochar	68.49	[64]
Iron-modified waste-biochar-sludge-based biochar	111.0	[25]
Egg shell-modified sludge biochar	154.18	[65]
Oyster shell-modified sludge biochar	129.03	[65]
Dolomite-modified sludge biochar	29.18	[66]

3.5. Adsorption Thermodynamics

The adsorption process is spontaneous and entails modifications of thermodynamic functions. To establish the spontaneity and nature of the adsorption process, we calculated the thermodynamic parameters Gibbs free energy, enthalpy change, and entropy change using the Van 't Hoff equation, and the obtained thermodynamic parameters are given in Table S2. As presented in Table S2, the reaction enthalpy (ΔH) was 954.963 kJ/mol, which suggests the rate of the endothermic phosphate adsorption process on the surface of the LaSBC. This parameter's positive and large value (>50 kJ mol^{-1}) implies that a chemical reaction underlies the adsorption process [56]. The free enthalpy of negative adsorption (ΔG) values means that phosphate adsorption onto the LaSBC occurred spontaneously. The positive values of ΔS indicated the increased unpredictability at the solid–liquid interface during adsorption. Thus, the adsorption of P ions on La-modified biochar is driven by entropy [67].

3.6. Adsorption and Desorption Studies

The stability and recyclability of adsorbents in the adsorption–desorption process are vital to the cost effectiveness of the adsorption process [6,56]. To assess the potential of the adsorbent for reuse in the subsequent phosphate adsorption study, 0.2 mol·L^{-1} NaCl was employed in desorption investigations. The adsorption capacity following desorption is shown in Figure S1, demonstrating a relatively stable adsorption capacity in six cycles. Specifically, 88.0% of the initial q_e was found to have been retained after the first desorption regeneration. The adsorption capacity after six cycles was 72.3% of the initial q_e, and it decreased by 15.7% in total. This trend could be due to the formation of La-P compounds and multilayer structures, saturating adsorption sites and preventing some sites from further adsorption [56]. The adsorption capacities of LaSBC remained above 70% after repeated adsorption and desorption, demonstrating that LaSBC is economical and practical for phosphate adsorption.

3.7. Dynamic Adsorption Studies

To evaluate the practical feasibility of LaSBC, continuous dynamic adsorption experiments were carried out on actual wastewater (P concentration of 3.08 mg/L) using a fixed-bed column. At the adsorbent dosages of 1 and 2 g, the breakthrough curves for

LaSBC are displayed in Figure S2. The effective treatment times of the adsorbent were 7.58 and 9.08 h, respectively, when the phosphate content in the effluent surpassed the current maximum permitted P concentration (0.5 mg·L^{-1}). The difference in time could be attributed to an increase in the amount of LaSBC, increasing the surface area of the adsorption layer and binding sites for phosphate adsorption [40]. The results showed that LaSBC had a long sustainable treatment time, which proves the feasibility of its practical application in polluted water.

3.8. Adsorption Mechanisms

Figure 9 illustrates the possible mechanisms underlying phosphate adsorption by LaSBC from an aqueous solution. The appearance of LaPO$_4$ peaks in the XRD of LaSBC-P suggests that LaPO$_4$ precipitation was one of the key processes for phosphate removal by LaSBC. La exhibits a strong affinity for phosphate because of the low Ksp value of LaPO$_4$ (3.7×10^{-23}) [29,68]. La produces complex compounds with PO$_4^{3-}$ ions, even at low concentrations in solutions [69]. Thus, precipitation serves as a crucial adsorption process for phosphate removal [29].
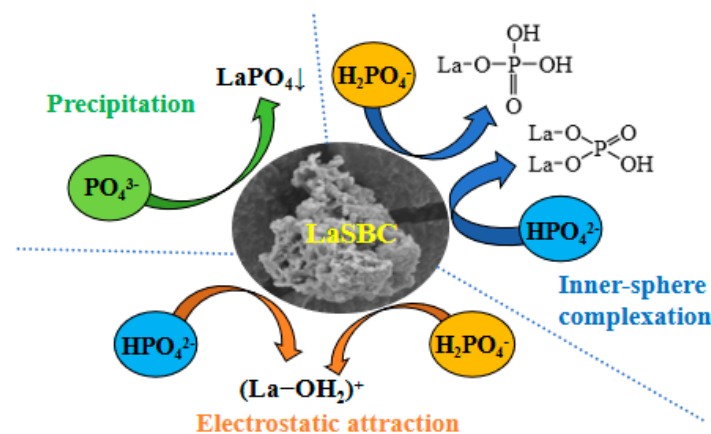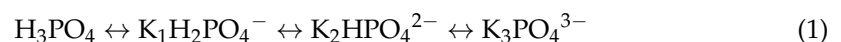

Figure 9. Possible mechanisms for phosphate adsorption on LaSBC.

The mechanism was further explained through the analysis of the types of phosphate at various pH levels and through determining the zero charge of LaSBC. The types of phosphate were varied at different pH levels, as shown in the following equation (Equation (1)) [51]:

$$H_3PO_4 \leftrightarrow K_1 H_2PO_4^- \leftrightarrow K_2 HPO_4^{2-} \leftrightarrow K_3 PO_4^{3-} \tag{1}$$

where $pK_1 = 2.13$, $pK_2 = 7.20$, and $pK_3 = 12.33$

Adsorbents containing metal are positively charged at low pH levels because metal hydroxides are readily protonated, and at high pH levels, they are negatively charged, as metal hydroxides are easily deprotonated under this condition [11,40,70]. As displayed in Figure 4b, pH$_{pzc}$ was 7.65 for LaSBC. The LaSBC was positively charged and protonated (La-OH + H$^+ \leftrightarrow$ La-OH^{2+}) at a pH of 2.0–7.65. This condition allowed the LaSBC to adsorb phosphate species H$_2$PO$_4^-$ or HPO$_4^{2-}$ through electrostatic attraction. In addition, in the pH range of 7.65–12.0, LaSBC was negatively charged and deprotonated. The adsorption of phosphate tended toward a lower pH, and the surface anion exchange process was followed by OH$^-$ release [71]. The solution pH rose as anion exchange advanced [11]. With an increase in pH, the effect of electrostatic attraction diminished rapidly.

However, hydroxyl groups present in the solution would undergo anion exchange with phosphate ions and form chemical bonds through inner-sphere complexation to achieve phosphate removal. Thus, anion exchange and inner-sphere complexation are inseparable from one another. FTIR and XPS measurements demonstrated that inner-sphere complexation was a key process in the phosphate removal process [16,36]. The FTIR spectra of LaSBC-P are displayed in Figure 2. The peak observed at approximately 621 and

538 cm^{-1} corresponded to the bending vibration of O-P-O, which proved that phosphate can be adsorbed effectively on adsorbents [69,72]. The peak noticed at 1399 cm^{-1} generated by –OH vibration was attenuated, evidently. This result might be caused by the exchange of –OH with phosphate to enable inner-sphere complexation [73].

The XPS spectra of LaSBC are displayed in Figure 4. The characteristic peaks of La 3d$_{5/2}$ for LaSBC were observed at 835.68 and 839.23 eV, and those of La 3d$_{3/2}$ were observed at 852.28 and 856.08 eV. After phosphate adsorption, the peaks of La 3d$_{5/2}$ were observed at 835.78 and 839.33 eV, whereas those of La 3d$_{3/2}$ were observed at 852.48 and 856.17 eV. The binding energies of La 3d$_{5/2}$ and 3d$_{3/2}$ shifted to higher values, which indicated a possible electron transfer in the valence band of La 3d and the occurrence of La-O-P inner-sphere complexation [16,35,74]. These results demonstrate that precipitation, electrostatic attraction, and inner-sphere complexation occurred during phosphate adsorption. These adsorption mechanisms are the same as several adsorption mechanisms reported in previous studies [75,76].

4. Conclusions

After the modification of lanthanum nitrate, the capability of LaSBC to remove phosphate from water considerably improved. The maximum experimental adsorption capacity for phosphate was 140.237 mg/g at pH 3.0. In addition, the adsorption mechanisms were predominantly precipitation, electrostatic attraction, and inner-sphere complexation. LaSBC possessed excellent recycling ability, and 72.3% of the initial q_e was found to have been retained after the sixth desorption cycle. The dynamic adsorption study revealed that the modified biochar has a long sustainable treatment period. Moreover, our findings prove the feasibility of biochar as an economical and efficient adsorbent for phosphate-polluted water. Future studies are expected to improve the effect of pH on LaSBC adsorption capacity.

Supplementary Materials: The following supporting information can be downloaded at https://www.mdpi.com/article/10.3390/su16135667/s1, Table S1: Kinetic parameters for the phosphate adsorption of the LaSBC; Table S2: Thermodynamic parameters for the phosphate adsorption of the LaSBC; Figure S1: Adsorption capacity after desorption of LaSBC; Figure S2: Effects of dosages on breakthrough point of LaSBC. Reference [77] is cited in Supplementary Materials.

Author Contributions: All authors contributed to the study conception and design. Conceptualization, methodology, and software were performed by Y.J. Writing—review and editing were performed by X.S. and H.Z. (Hongxia Zhang). Investigation, resources, and methodology were performed by Q.L. Supervision was performed by J.M., M.X., B.D. and H.Z. (Hongxiang Zhu). The first draft of the manuscript was written by Y.J. and all authors commented on previous versions of the manuscript. All authors have read and agreed to the published version of the manuscript.

Data Availability Statement: The datasets used or analyzed during the current study are available from the corresponding author upon reasonable request.

Conflicts of Interest: The authors declare that they have no known competing financial interests or personal relationships that could have appeared to influence the work reported in this paper.

References

1. Sun, J.; Yang, Q.; Wang, D.; Wang, S.; Chen, F.; Zhong, Y.; Yi, K.; Yao, F.; Jiang, C.; Li, S.; et al. Nickel toxicity to the performance and microbial community of enhanced biological phosphorus removal system. *Chem. Eng. J.* **2017**, *313*, 415–423. [CrossRef]
2. Wang, D.; Yang, G.; Li, X.; Zheng, W.; Wu, Y.; Yang, Q.; Zeng, G. Inducing mechanism of biological phosphorus removal driven by the aerobic/extended-idle regime. *Biotechnol. Bioeng.* **2012**, *109*, 2798–2807. [CrossRef] [PubMed]
3. Xu, Q.; Liu, X.; Wang, D.; Wu, Y.; Wang, Q.; Liu, Y.; Li, X.; An, H.; Zhao, J.; Chen, F.; et al. Free ammonia-based pretreatment enhances phosphorus release and recovery from waste activated sludge. *Chemosphere* **2018**, *213*, 276–284. [CrossRef]

4. Mayer, B.K.; Baker, L.A.; Boyer, T.H.; Drechsel, P.; Gifford, M.; Hanjra, M.A.; Parameswaran, P.; Stoltzfus, J.; Westerhoff, P.; Rittmann, B.E. Total Value of Phosphorus Recovery. *Environ. Sci. Technol.* **2016**, *50*, 6606–6620. [CrossRef] [PubMed]

5. Shang, Y.; Xu, X.; Qi, S.; Zhao, Y.; Ren, Z.; Gao, B. Preferable uptake of phosphate by hydrous zirconium oxide nanoparticles embedded in quaternary-ammonium Chinese reed. *J. Colloid Interface Sci.* **2017**, *496*, 118–129. [CrossRef] [PubMed]

6. Jung, K.-W.; Lee, S.; Lee, Y.J. Synthesis of novel magnesium ferrite ($MgFe_2O_4$)/biochar magnetic composites and its adsorption behavior for phosphate in aqueous solutions. *Bioresour. Technol.* **2017**, *245*, 751–759. [CrossRef] [PubMed]

7. Xie, T.; Mo, C.; Li, X.; Zhang, J.; An, H.; Yang, Q.; Wang, D.; Zhao, J.; Zhong, Y.; Zeng, G. Effects of different ratios of glucose to acetate on phosphorus removal and microbial community of enhanced biological phosphorus removal (EBPR) system. *Environ. Sci. Pollut. Res.* **2017**, *24*, 4494–4505. [CrossRef] [PubMed]

8. Wu, Y.; Li, X.; Yang, Q.; Wang, D.; Xu, Q.; Yao, F.; Chen, F.; Tao, Z.; Huang, X. Hydrated lanthanum oxide-modified diatomite as highly efficient adsorbent for low-concentration phosphate removal from secondary effluents. *J. Environ. Manag.* **2019**, *231*, 370–379. [CrossRef] [PubMed]

9. Huang, W.; Yu, X.; Tang, J.; Zhu, Y.; Zhang, Y.; Li, D. Enhanced adsorption of phosphate by flower-like mesoporous silica spheres loaded with lanthanum. *Microporous Mesoporous Mater.* **2015**, *217*, 225–232. [CrossRef]

10. Zhang, M.; Song, G.; Gelardi, D.L.; Huang, L.; Khan, E.; Mašek, O.; Parikh, S.J.; Ok, Y.S. Evaluating biochar and its modifications for the removal of ammonium, nitrate, and phosphate in water. *Water Res.* **2020**, *186*, 116303. [CrossRef]

11. Xu, Q.; Chen, Z.; Wu, Z.; Xu, F.; Yang, D.; He, Q.; Li, G.; Chen, Y. Novel lanthanum doped biochars derived from lignocellulosic wastes for efficient phosphate removal and regeneration. *Bioresour. Technol.* **2019**, *289*, 121600. [CrossRef] [PubMed]

12. Yang, S.; Jin, P.; Wang, X.; Zhang, Q.; Chen, X. Phosphate recovery through adsorption assisted precipitation using novel precipitation material developed from building waste: Behavior and mechanism. *Chem. Eng. J.* **2016**, *292*, 246–254. [CrossRef]

13. Shang, Y.; Kan, Y.; Xu, X. Stability and regeneration of metal catalytic sites with different sizes in Fenton-like system. *Chin. Chem. Lett.* **2023**, *34*, 108278. [CrossRef]

14. Shrestha, R.; Ban, S.; Devkota, S.; Sharma, S.; Joshi, R.; Tiwari, A.P.; Kim, H.Y.; Joshi, M.K. Technological trends in heavy metals removal from industrial wastewater: A review. *J. Environ. Chem. Eng.* **2021**, *9*, 105688. [CrossRef]

15. Li, R.; Wang, J.J.; Zhou, B.; Awasthi, M.K.; Ali, A.; Zhang, Z.; Lahori, A.H.; Mahar, A. Recovery of phosphate from aqueous solution by magnesium oxide decorated magnetic biochar and its potential as phosphate-based fertilizer substitute. *Bioresour. Technol.* **2016**, *215*, 209–214. [CrossRef] [PubMed]

16. Qiu, H.; Liang, C.; Yu, J.; Zhang, Q.; Song, M.; Chen, F. Preferable phosphate sequestration by nano-La(III) (hydr)oxides modified wheat straw with excellent properties in regeneration. *Chem. Eng. J.* **2017**, *315*, 345–354. [CrossRef]

17. Biswas, B.K.; Inoue, K.; Ghimire, K.N.; Harada, H.; Ohto, K.; Kawakita, H. Removal and recovery of phosphorus from water by means of adsorption onto orange waste gel loaded with zirconium. *Bioresour. Technol.* **2008**, *99*, 8685–8690. [CrossRef] [PubMed]

18. Lu, S.; Bai, S.; Shan, H. Mechanisms of phosphate removal from aqueous solution by blast furnace slag and steel furnace slag. *J. Zhejiang Univ.-Sci. A* **2008**, *9*, 125–132. [CrossRef]

19. Chen, Y.; Wang, R.; Duan, X.; Wang, S.; Ren, N.; Ho, S.-H. Production, properties, and catalytic applications of sludge derived biochar for environmental remediation. *Water Res.* **2020**, *187*, 116390. [CrossRef] [PubMed]

20. Wu, Q.; Bao, X.; Guo, W.; Wang, B.; Li, Y.; Luo, H.; Wang, H.; Ren, N. Medium chain carboxylic acids production from waste biomass: Current advances and perspectives. *Biotechnol. Adv.* **2019**, *37*, 599–615. [CrossRef]

21. Chen, Y.; Ho, S.-H.; Nagarajan, D.; Ren, N.; Chang, J.-S. Waste biorefineries—Integrating anaerobic digestion and microalgae cultivation for bioenergy production. *Curr. Opin. Biotechnol.* **2018**, *50*, 101–110. [CrossRef] [PubMed]

22. Chen, Y.; Li, S.; Ho, S.-H.; Wang, C.; Lin, Y.-C.; Nagarajan, D.; Chang, J.-S.; Ren, N. Integration of sludge digestion and microalgae cultivation for enhancing bioenergy and biorefinery. *Renew. Sustain. Energy Rev.* **2018**, *96*, 76–90. [CrossRef]

23. Chen, Y.; Yang, Z.; Ren, N.; Ho, S.-H. Optimizing the production of short and medium chain fatty acids (SCFAs and MCFAs) from waste activated sludge using different alkyl polyglucose surfactants, through bacterial metabolic analysis. *J. Hazard. Mater.* **2020**, *384*, 121384. [CrossRef] [PubMed]

24. Huang, Y.; Xia, S.; Lyu, J.; Tang, J. Highly efficient removal of aqueous Hg^{2+} and CH_3Hg^+ by selective modification of biochar with 3-mercaptopropyltrimethoxysilane. *Chem. Eng. J.* **2019**, *360*, 1646–1655. [CrossRef]

25. Yang, Q.; Wang, X.; Luo, W.; Sun, J.; Xu, Q.; Chen, F.; Zhao, J.; Wang, S.; Yao, F.; Wang, D.; et al. Effectiveness and mechanisms of phosphate adsorption on iron-modified biochars derived from waste activated sludge. *Bioresour. Technol.* **2018**, *247*, 537–544. [CrossRef] [PubMed]

26. Zama, E.F.; Li, G.; Tang, Y.-T.; Reid, B.J.; Ngwabie, N.M.; Sun, G.-X. The removal of arsenic from solution through biochar-enhanced precipitation of calcium-arsenic derivatives. *Environ. Pollut.* **2022**, *292*, 118241. [CrossRef] [PubMed]

27. Yin, Q.; Liu, M.; Ren, H. Biochar produced from the co-pyrolysis of sewage sludge and walnut shell for ammonium and phosphate adsorption from water. *J. Environ. Manag.* **2019**, *249*, 109410. [CrossRef] [PubMed]

28. Yin, Q.; Liu, M.; Li, Y.; Li, H.; Wen, Z. Computational study of phosphate adsorption on Mg/Ca modified biochar structure in aqueous solution. *Chemosphere* **2021**, *269*, 129374. [CrossRef] [PubMed]

29. Liao, T.; Li, T.; Su, X.; Yu, X.; Song, H.; Zhu, Y.; Zhang, Y. La(OH)$_3$-modified magnetic pineapple biochar as novel adsorbents for efficient phosphate removal. *Bioresour. Technol.* **2018**, *263*, 207–213. [CrossRef]

30. He, J.; Wang, W.; Sun, F.; Shi, W.; Qi, D.; Wang, K.; Shi, R.; Cui, F.; Wang, C.; Chen, X. Highly Efficient Phosphate Scavenger Based on Well-Dispersed La(OH)₃ Nanorods in Polyacrylonitrile Nanofibers for Nutrient-Starvation Antibacteria. *ACS Nano* **2015**, *9*, 9292–9302. [CrossRef]

31. Liu, B.; Nan, J.; Zu, X.; Zhang, X.; Huang, W.; Wang, W. La-based-adsorbents for efficient biological phosphorus treatment of wastewater: Synergistically strengthen of chemical and biological removal. *Chemosphere* **2020**, *255*, 127010. [CrossRef] [PubMed]

32. Yu, J.; Xiang, C.; Zhang, G.; Wang, H.; Ji, Q.; Qu, J. Activation of Lattice Oxygen in LaFe (Oxy)hydroxides for Efficient Phosphorus Removal. *Environ. Sci. Technol.* **2019**, *53*, 9073–9080. [CrossRef] [PubMed]

33. Li, R.; Wang, J.J.; Gaston, L.A.; Zhou, B.; Li, M.; Xiao, R.; Wang, Q.; Zhang, Z.; Huang, H.; Liang, W.; et al. An overview of carbothermal synthesis of metal–biochar composites for the removal of oxyanion contaminants from aqueous solution. *Carbon* **2018**, *129*, 674–687. [CrossRef]

34. Fang, L.; Liu, R.; Li, J.; Xu, C.; Huang, L.-Z.; Wang, D. Magnetite/Lanthanum hydroxide for phosphate sequestration and recovery from lake and the attenuation effects of sediment particles. *Water Res.* **2018**, *130*, 243–254. [CrossRef] [PubMed]

35. Min, X.; Wu, X.; Shao, P.; Ren, Z.; Ding, L.; Luo, X. Ultra-high capacity of lanthanum-doped UiO-66 for phosphate capture: Unusual doping of lanthanum by the reduction of coordination number. *Chem. Eng. J.* **2019**, *358*, 321–330. [CrossRef]

36. Wang, Z.; Shen, D.; Shen, F.; Li, T. Phosphate adsorption on lanthanum loaded biochar. *Chemosphere* **2016**, *150*, 1–7. [CrossRef] [PubMed]

37. Jin, J.; Li, Y.; Zhang, J.; Wu, S.; Cao, Y.; Liang, P.; Zhang, J.; Wong, M.H.; Wang, M.; Shan, S.; et al. Influence of pyrolysis temperature on properties and environmental safety of heavy metals in biochars derived from municipal sewage sludge. *J. Hazard. Mater.* **2016**, *320*, 417–426. [CrossRef] [PubMed]

38. Li, J.; Li, B.; Huang, H.; Zhao, N.; Zhang, M.; Cao, L. Investigation into lanthanum-coated biochar obtained from urban dewatered sewage sludge for enhanced phosphate adsorption. *Sci. Total Environ.* **2020**, *714*, 136839. [CrossRef] [PubMed]

39. Guo, J.; Chen, B. Insights on the Molecular Mechanism for the Recalcitrance of Biochars: Interactive Effects of Carbon and Silicon Components. *Environ. Sci. Technol.* **2014**, *48*, 9103–9112. [CrossRef]

40. Jia, Z.; Zeng, W.; Xu, H.; Li, S.; Peng, Y. Adsorption removal and reuse of phosphate from wastewater using a novel adsorbent of lanthanum-modified platanus biochar. *Process Saf. Environ. Prot.* **2020**, *140*, 221–232. [CrossRef]

41. Li, X.; Liu, W.; Zhang, J.; Wang, Z.; Guo, Z.; Ali, J.; Wang, L.; Yu, Z.; Zhang, X.; Sun, Y. Effective removal of microplastics by filamentous algae and its magnetic biochar: Performance and mechanism. *Chemosphere* **2024**, *358*, 142152. [CrossRef]

42. Fan, J.; Li, Y.; Yu, H.; Li, Y.; Yuan, Q.; Xiao, H.; Li, F.; Pan, B. Using sewage sludge with high ash content for biochar production and Cu(II) sorption. *Sci. Total Environ.* **2020**, *713*, 136663. [CrossRef] [PubMed]

43. Pasumarthi, R.; Sawargaonkar, G.; Kale, S.; Kumar, N.V.; Choudhari, P.L.; Singh, R.; Davala, M.S.; Rani, C.S.; Mutnuri, S.; Jat, M.L. Innovative bio-pyrolytic method for efficient biochar production from maize and pigeonpea stalks and their characterization. *J. Clean. Prod.* **2024**, *448*, 141573. [CrossRef]

44. Qian, G.; Xu, L.; Li, N.; Wang, K.; Qu, Y.; Xu, Y. Enhanced arsenic migration in tailings soil with the addition of humic acid, fulvic acid and thiol-modified humic acid. *Chemosphere* **2022**, *286*, 131784. [CrossRef]

45. Yu, H.; Zhang, D.; Gu, L.; Wen, H.; Zhu, N. Coupling sludge-based biochar and electrolysis for conditioning and dewatering of sewage sludge: Effect of char properties. *Environ. Res.* **2022**, *214*, 113974. [CrossRef]

46. Chen, L.; Li, Y.; Sun, Y.; Chen, Y.; Qian, J. La(OH)₃ loaded magnetic mesoporous nanospheres with highly efficient phosphate removal properties and superior pH stability. *Chem. Eng. J.* **2019**, *360*, 342–348. [CrossRef]

47. Xiao, Y.-F.; Zhang, Y.; Wang, D.-C.; Su, Y.-M.; Wu, J.; Liu, J.-Q.; Yang, L.-L.; Jin, Z. Hydrothermal synthesis of lanthanum oxide nanoparticles modified pumice: High lanthanum oxide loading ratio and efficiency phosphate removal. *J. Environ. Chem. Eng.* **2024**, *12*, 111587. [CrossRef]

48. Chen, K.; Guo, S.; Zeng, Y.; Huang, W.; Peng, J.; Zhang, L.; Yin, S. Facile preparation and characterization of lanthanum oxide powders by the calcination of lanthanum carbonate hydrate in microwave field. *Ceram. Int.* **2020**, *46*, 165–170. [CrossRef]

49. Li, L.; Jiang, W.; Pan, H.; Xu, X.; Tang, Y.; Ming, J.; Xu, Z.; Tang, R. Improved Luminescence of Lanthanide(III)-Doped Nanophosphors by Linear Aggregation. *J. Phys. Chem. C* **2007**, *111*, 4111–4115. [CrossRef]

50. Shan, S.; Chen, Z.; Yuen Koh, K.; Cui, F.; Paul Chen, J. Development and application of lanthanum peroxide loaded sepiolite nanocomposites for simultaneous removal of phosphate and inhibition of cyanobacteria growth. *J. Colloid Interface Sci.* **2022**, *624*, 691–703. [CrossRef]

51. Tang, Q.; Shi, C.; Shi, W.; Huang, X.; Ye, Y.; Jiang, W.; Kang, J.; Liu, D.; Ren, Y.; Li, D. Preferable phosphate removal by nano-La(III) hydroxides modified mesoporous rice husk biochars: Role of the host pore structure and point of zero charge. *Sci. Total Environ.* **2019**, *662*, 511–520. [CrossRef]

52. Li, S.; Luo, C.; Yan, F.; Yang, Y.; Guo, B.; Wang, L.; Xu, S.; Wu, F.; Ji, P. Remediation of Pb(II) and Cd(II) in polluted waters with calcium thioglycolate–modified straw biochar. *Environ. Pollut.* **2023**, *338*, 122638. [CrossRef]

53. Goscianska, J.; Ptaszkowska-Koniarz, M.; Frankowski, M.; Franus, M.; Panek, R.; Franus, W. Removal of phosphate from water by lanthanum-modified zeolites obtained from fly ash. *J. Colloid Interface Sci.* **2018**, *513*, 72–81. [CrossRef]

54. Zhang, J.; Shen, Z.; Shan, W.; Chen, Z.; Mei, Z.; Lei, Y.; Wang, W. Adsorption behavior of phosphate on Lanthanum(III) doped mesoporous silicates material. *J. Environ. Sci.* **2010**, *22*, 507–511. [CrossRef] [PubMed]

55. Wang, Z.; Guo, H.; Shen, F.; Yang, G.; Zhang, Y.; Zeng, Y.; Wang, L.; Xiao, H.; Deng, S. Biochar produced from oak sawdust by Lanthanum (La)-involved pyrolysis for adsorption of ammonium (NH^{4+}), nitrate (NO^{3-}), and phosphate (PO_4^{3-}). *Chemosphere* **2015**, *119*, 646–653. [CrossRef] [PubMed]

56. Aryee, A.A.; Mpatani, F.M.; Zhang, X.; Kani, A.N.; Dovi, E.; Han, R.; Li, Z.; Qu, L. Iron (III) and iminodiacetic acid functionalized magnetic peanut husk for the removal of phosphate from solution: Characterization, kinetic and equilibrium studies. *J. Clean. Prod.* **2020**, *268*, 122191. [CrossRef]

57. Yin, Q.; Wang, R.; Zhao, Z. Application of Mg–Al-modified biochar for simultaneous removal of ammonium, nitrate, and phosphate from eutrophic water. *J. Clean. Prod.* **2018**, *176*, 230–240. [CrossRef]

58. Jang, H.M.; Yoo, S.; Choi, Y.-K.; Park, S.; Kan, E. Adsorption isotherm, kinetic modeling and mechanism of tetracycline on Pinus taeda-derived activated biochar. *Bioresour. Technol.* **2018**, *259*, 24–31. [CrossRef]

59. Cui, X.; Dai, X.; Khan, K.Y.; Li, T.; Yang, X.; He, Z. Removal of phosphate from aqueous solution using magnesium-alginate/chitosan modified biochar microspheres derived from Thalia dealbata. *Bioresour. Technol.* **2016**, *218*, 1123–1132. [CrossRef]

60. Yang, H.I.; Lou, K.; Rajapaksha, A.U.; Ok, Y.S.; Anyia, A.O.; Chang, S.X. Adsorption of ammonium in aqueous solutions by pine sawdust and wheat straw biochars. *Environ. Sci. Pollut. Res.* **2018**, *25*, 25638–25647. [CrossRef]

61. Qu, J.; Akindolie, M.S.; Feng, Y.; Jiang, Z.; Zhang, G.; Jiang, Q.; Deng, F.; Cao, B.; Zhang, Y. One-pot hydrothermal synthesis of $NaLa(CO_3)_2$ decorated magnetic biochar for efficient phosphate removal from water: Kinetics, isotherms, thermodynamics, mechanisms and reusability exploration. *Chem. Eng. J.* **2020**, *394*, 124915. [CrossRef]

62. Meng, J.; Feng, X.; Dai, Z.; Liu, X.; Wu, J.; Xu, J. Adsorption characteristics of Cu(II) from aqueous solution onto biochar derived from swine manure. *Environ. Sci. Pollut. Res.* **2014**, *21*, 7035–7046. [CrossRef] [PubMed]

63. Liu, Z.; Liu, H.; Zhang, Y.; Lichtfouse, E. Efficient phosphate recycling by adsorption on alkaline sludge biochar. *Environ. Chem. Lett.* **2023**, *21*, 21–30. [CrossRef]

64. Wang, Z.; Miao, R.; Ning, P.; He, L.; Guan, Q. From wastes to functions: A paper mill sludge-based calcium-containing porous biochar adsorbent for phosphorus removal. *J. Colloid Interface Sci.* **2021**, *593*, 434–446. [CrossRef]

65. Li, J.; Cao, L.; Li, B.; Huang, H.; Yu, W.; Sun, C.; Long, K.; Young, B. Utilization of activated sludge and shell wastes for the preparation of Ca-loaded biochar for phosphate removal and recovery. *J. Clean. Prod.* **2023**, *382*, 135395. [CrossRef]

66. Li, J.; Li, B.; Huang, H.; Lv, X.; Zhao, N.; Guo, G.; Zhang, D. Removal of phosphate from aqueous solution by dolomite-modified biochar derived from urban dewatered sewage sludge. *Sci. Total Environ.* **2019**, *687*, 460–469. [CrossRef]

67. Cegłowski, M.; Schroeder, G. Preparation of porous resin with Schiff base chelating groups for removal of heavy metal ions from aqueous solutions. *Chem. Eng. J.* **2015**, *263*, 402–411. [CrossRef]

68. Yang, J.; Zhou, L.; Zhao, L.; Zhang, H.; Yin, J.; Wei, G.; Qian, K.; Wang, Y.; Yu, C. A designed nanoporous material for phosphate removal with high efficiency. *J. Mater. Chem.* **2011**, *21*, 2489. [CrossRef]

69. Wang, Z.; Wang, H.; Li, Q.; Xu, M.; Guo, Y.; Li, J.; Wu, T. pH effect on Re(VII) and Se(IV) diffusion in compacted GMZ bentonite. *Appl. Geochem.* **2016**, *73*, 1–7. [CrossRef]

70. Xiong, W.; Tong, J.; Yang, Z.; Zeng, G.; Zhou, Y.; Wang, D.; Song, P.; Xu, R.; Zhang, C.; Cheng, M. Adsorption of phosphate from aqueous solution using iron-zirconium modified activated carbon nanofiber: Performance and mechanism. *J. Colloid Interface Sci.* **2017**, *493*, 17–23. [CrossRef]

71. Hiemstra, T.; Van Riemsdijk, W.H. Surface Structural Ion Adsorption Modeling of Competitive Binding of Oxyanions by Metal (Hydr)oxides. *J. Colloid Interface Sci.* **1999**, *210*, 182–193. [CrossRef]

72. Zhang, L.; Zhou, Q.; Liu, J.; Chang, N.; Wan, L.; Chen, J. Phosphate adsorption on lanthanum hydroxide-doped activated carbon fiber. *Chem. Eng. J.* **2012**, *185–186*, 160–167. [CrossRef]

73. Chen, Y.; Xu, R.; Li, Y.; Liu, Y.; Wu, Y.; Chen, Y.; Zhang, J.; Chen, S.; Yin, H.; Zeng, Z.; et al. $La(OH)_3$-modified magnetic $CoFe_2O_4$ nanocomposites: A novel adsorbent with highly efficient activity and reusability for phosphate removal. *Colloids Surf. A Physicochem. Eng. Asp.* **2020**, *599*, 124870. [CrossRef]

74. Wu, B.; Fang, L.; Fortner, J.D.; Guan, X.; Lo, I.M.C. Highly efficient and selective phosphate removal from wastewater by magnetically recoverable $La(OH)_3/Fe_3O_4$ nanocomposites. *Water Res.* **2017**, *126*, 179–188. [CrossRef]

75. Mahmoud, A.S.; Mostafa, M.K.; Nasr, M. Regression model, artificial intelligence, and cost estimation for phosphate adsorption using encapsulated nanoscale zero-valent iron. *Sep. Sci. Technol.* **2019**, *54*, 13–26. [CrossRef]

76. Zhang, Y.; Pan, B. Modeling batch and column phosphate removal by hydrated ferric oxide-based nanocomposite using response surface methodology and artificial neural network. *Chem. Eng. J.* **2014**, *249*, 111–120. [CrossRef]

77. Qi, G.; Pan, Z.; Zhang, X.; Chang, S.; Wang, H.; Wang, M.; Xiang, W.; Gao, B. Microwave biochar produced with activated carbon catalyst: Characterization and adsorption of heavy metals. *Environ. Res.* **2023**, *216*, 114732. [CrossRef]